

Axillary Artery Diameter Measurement using Wiener Filtered Smoothing Technique

Eko Supriyanto, Lai Khin Wee, Rino Ferdian Surakusumah

Abstract-- The axillary brachial plexus nerve block provides excellent surgical anesthesia for the elbow, forearm, and hand. By using the ultrasound scanning technique, researchers can identify the location of the axillary artery during the surgery and perform clinical analysis on physiological effect of nerve block by measuring the diameter of the axillary artery. However, manual assessment and measurement of the ultrasound image can be inaccurate, restricted to intra and inter observer variability and time consuming. The objective of this paper is to increase the resolution of the image to propose a precise axillary artery diameter measurement method by Wiener filter. The resolution of images are compared by using Wiener, Frost and followed by anisotropic diffusion filters. Manual thresholding is applied to the image and followed by level set segmentation. The precision of the artery measurement before and after the image processing techniques is gauged by evaluating the standard deviation of the diameter parameters. The findings show that the measured diameter of processed image has smaller standard deviation of 0.019 mm as compared with original image of 0.045 mm. The study concludes that the processed image can clearly indicate the location of the axillary artery.

Keywords -- Ultrasound, Axillary Block Imaging, Speckle Noise, Image Smoothing, Morphological Process, Axillary Artery Diameter

I. INTRODUCTION

THE brachial plexus nerve controls the nerve network from throat to the upper limb. After the brachial nerve passes through neck and shoulder, its three cords are divided into numerous terminal nerves. Some of these nerves, namely, musculocutaneous, median, ulna, radial and axillary nerve serve as vital element in the nerve block and supply the sensory and motor innervations to the whole upper extremity [1].

A nerve block or regional anaesthesia is an injection of anaesthetic precisely adjacent to a major nerve by using a needle of length between 1.5 inches to 6 inches. The anaesthetic will stop the innervations supply from that point to the terminal end of the nerve. Surprisingly, a block may not be

adjacent to the targeted area but can cause everything "downstream" from where the block was performed to be numb. The regional nerve block is different from general anaesthesia. General anaesthesia is a widely known practice and involves the injection of the anaesthetic directly to the body area where the effect of anaesthetic is partially required, making it more localised. Besides, the general anaesthetic will have a shorter period of effect as compared with nerve block and is a less effective anaesthesia method [7].

Both magnetic resonance imaging (MRI) and computed tomography scanning (CT scan) produce clear anatomical images of the brachial plexus [8] and CT scan takes only about 5 minute for completion. But these two techniques are expensive and inaccessible to the operating room [2], making it unsuitable for nerve block anaesthetic procedures. Moreover, CT scan exposes patient to the risk of radiation, causing harm and damage to body tissue if it is not handled properly.

Fluoroscopy is another alternative to the MRI and CT scan. However, it provides excellent visualization of bony landmarks instead of nerve and blood vessels. Moreover, the contrast dye spreads near to the neurovascular bundle within the plexus sheath. These shortcomings make fluoroscopy a less favourable visualization method in the nerve block technique.

Ultrasound, on the other hand, is non-invasive, portable, and moderately priced [3] modality. The ultrasound transducer emits high frequency sound waves (ranged between 1 to 5 MHz) into subject body and travel back to the transducer. The reflected waves are relayed to machine and have their distance from probe to tissue or organ and back to probe calculated. During the scanning process, no radiation hazard has been exposed to the patient and it is easy to be used by the clinician [9]. The scanning process normally takes a moderate duration of 10 to 15 minutes.

Due to the versatility of ultrasound scanning, ultrasound guided plexus brachial nerve block has been gaining popularity as the preferred nerve block surgical scanning technique in medical anaesthesia field. Ultrasound scanning is conducted at the axillary region before and during the nerve block procedure is carried out by the anaesthesiologist. The transducer is situated strategically at the armpit region to detect the axillary artery, which provides guidance for needle insertion [10].

There have been many well established medical researches which are conducted to study the advantages of the ultrasound guided nerve block. A study by Schwemmer [11] concluded

This work was supported in part by the Universiti Teknologi Malaysia, Skudai UTM, Malaysia.

Supriyanto, E is with the Head Department of Clinical Science and Engineering, and Advanced Diagnostics and E-Health Research Group, Universiti Teknologi Malaysia, Skudai UTM, Malaysia (e-mail: eko@utm.my).

K. W. Lai is with the Biotechnology Research Alliance, and Advanced Diagnostics and E-Health Research Group, Faculty of Bioscience and Medical Engineering, Universiti Teknologi Malaysia, Skudai UTM, Malaysia (e-mail: laikw2@gmail.com).

F. S. Rino is with Department of Clinical Science and Engineering, Faculty of Bioscience and Medical Engineering, Universiti Teknologi Malaysia (e-mail: rinoferdian@gmail.com).

that axillary brachial plexus blocks have a higher success rate when using ultrasound scanning instead of nerve stimulation. Chan [11] showed that there was no increase of success rate with the addition of nerve stimulation. Another study by Casati [11] has claimed that the sensory block performs faster with ultrasound.

The axillary artery is classified as large and elastic blood vessel but has a smaller diameter than axillary vein. The axillary artery carries the oxygenated blood to the thorax, axillary and upper limb region of human body. The axillary vein is larger than the axillary artery, as shown in fig. 1, and can carry more deoxygenated blood than axillary artery. Axillary vein is located superior to the axillary artery. The axillary vein has valve along the way in order to prevent possible reverse flow of the deoxygenated blood.

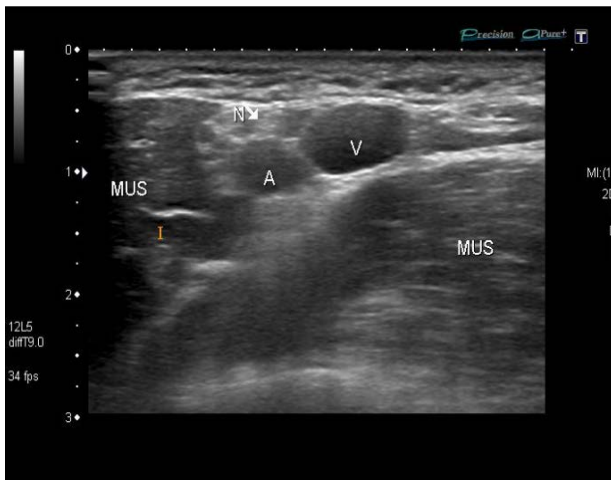


Fig. 1 Axillary artery (A) and axillary vein (V)

The determination of the axillary artery location is an important element before the ultrasound guided axillary nerve block procedures because the ulna, radial, median and musculocutaneous nerves are located surrounding the axillary artery. The median nerve is located superficial and slightly cephalic to the artery, the radial artery is located deep to the artery and the ulna nerve is located caudad to the artery [1]. By locating the axillary artery, anaesthesiologist can insert the needle fill with anaesthesia (to prevent air bubble) to the surrounding area of the targeted nerve.

Previous studies have measured axillary artery diameter using ultrasound image because the variations of the axillary artery diameter serves as a significant clinical parameter for assessing the effect of the nerve block on the blood pressure on the axillary artery, the changing pattern of blood flow affected by the various volume of anaesthetic during nerve block procedure [12] and arterial stiffness [13]. A similar clinical research has been conducted on the effect of the median nerve block on the radial artery diameter and peak velocity. The study concluded that there has been obvious increase in the peak velocities after the nerve blockage has been carried out [14]. Although the ultrasound technique has been championed as the better option compared to other scanning techniques, the ultrasound images have shown

limitation in providing clear visualisation of the location of axillary artery since the ultrasound images are contaminated by the speckle noise and artefacts [15]. The presences of noise and artefacts cause taking measurements manually from the ultrasound images lacks persistency.

The unwanted muscle, soft tissue and fatty cysts can be easily scanned in axillary region but the axillary artery and vein is difficult to be located precisely. Sometimes the ultrasound transducer exerts pressure on the axillary blood vessels, causing the collapse of the blood vessel and creates confusion for the inexperienced sonographer. As a result, assessing the ultrasound image may rely heavily on training and experience of the sonographer and can lead to the lacking accuracy.

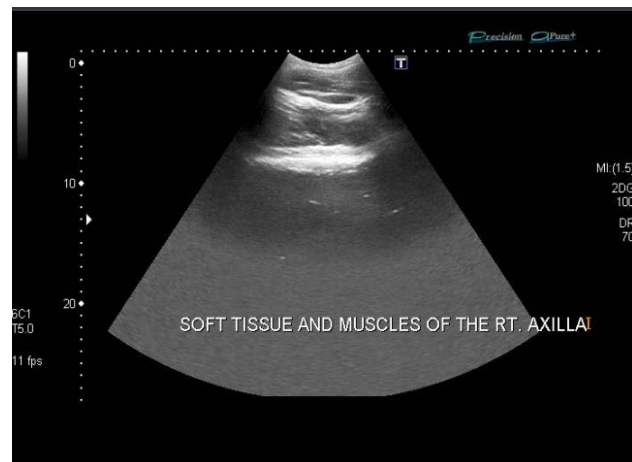


Fig. 2 Soft tissue and muscles of axillary region

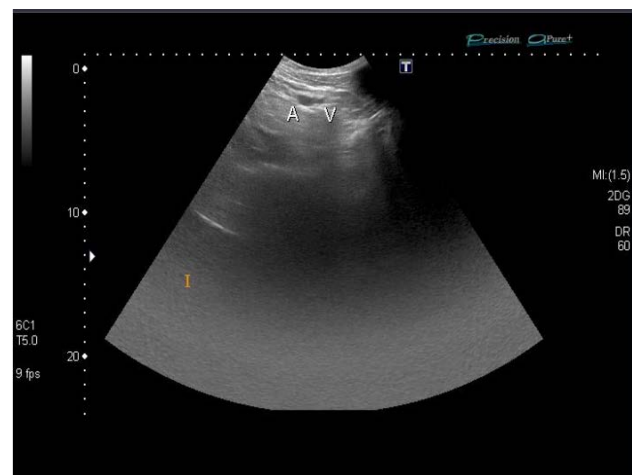


Fig. 3 Obscure axillary artery and vein image

Thus, technical image processing plays significant role in providing reliable visualization and assessment for the anaesthesiologists, sonographers and researchers. Some common practices in processing the ultrasound images include smoothing the image to reduce speckle noise using filters, applying the edge detection method to preserve the lines and edges of the image objects and segmentation methods to retain the desired image object and eliminate other unwanted elements. The smoothing process removes the contaminants

from the ultrasound image by using filters to single out high frequency components. Common filters in smoothing ultrasound image include Gabon filter, median filter, Lee filter, Kaun filter, and Wiener filter. The loss of signals information has been the main concern when smoothing the ultrasound image.

A study on the performance of various filters such as Anisotropic diffusion filter, Wavelet filter, Kaun filter, Weiner filter, Median filter and Lee filter has shown that noises have been reduced considerably in the ultrasound image of this experiment and the Wavelet filter showed a greater significance in clearing the image's noise [6]. Another study by Su and Seung [15] concluded that the wavelet filter has been a better filter than Wiener filter since the wavelet filter showed superior edge and feature selectivity in passing certain high frequency data. Another experiment by Vanithamani, Umamaheswari and Ezhilarasi [16] showed that Lee filter has been batter than Kaun and Frost filter while the median filter was the worst among the filters compared.

Segmentation improves the phases of measurement and diagnosis by segmenting the image to show only wanted image characters [4, 6] and using edge detection to outline the shape of the image objects. However, all these processing methods need to be tested by trial and error to evaluate the outcome of each method in searching for the best processing techniques combination. Several segmentation techniques have been explored in previous studies. The most celebrating region based image segmentation model was developed by Mumford and Shah [5]. The shortcoming of this technique lied with difficulties in numerical computation [5]. An approach has been introduced by Ambrosio and Tortorelli but their segmentation algorithm failed to produce an efficient segmentation result on images with noise, artefacts, and faced the problem of losing image information [5]. Another segmentation method, Snake or Active Contour Models failed to prove as an effective segmentation system given this method required the help of user to initiate the snake [24].

In a similar study on improving the brachial artery diameter, Vincenzo [13] has proposed the use of a system to analyse the ultrasound image based on a robust edge detection algorithm. However, manual intervention was still a necessity in case the contour tracking algorithm was not performing. The morphological method is a segmentation method which separates the image object from the image background and refines the shape of the object [17]. This image processing technique highlights the importance of geometry structure in removing the background image by applying the morphological theory [18].

The objective of this project is to measure the diameter of the axillary artery diameter by using enhanced ultrasound image for its precision. No study has been carried out on the precision of the diameter parameter of original and enhanced images before. The standard deviation will be used as a gauge for the measurement consistency. However, the final result may not be significantly reliable enough due to the limited number of subject and images.

II. METHODOLOGY

In this project, a Toshiba 8 MHz linear transducer has been utilised. Transverse plane scanning is chosen as this plane gives the best view of axillary brachial plexus region. The ultrasound scanning machine uses the 2D B mode scanning to collect the axillary images and one subject has been selected to do the scanning. We have tested various filters to smooth the images and the image's peak signals to noise ratios (PSNR) are calculated. After that, Otsu's method and manual thresholding are tested to segment the image. Diameter of artery before and after enhancement are measured and compared.

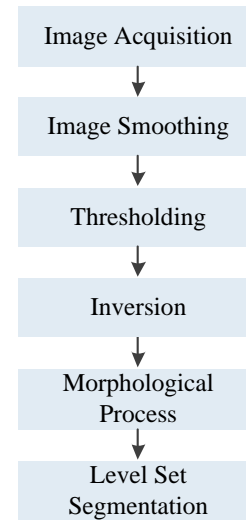


Fig. 4 Methodology block diagram

A. Image Acquisitions

Ultrasound scanning gives graphical visualisation of the plexus brachial nerve, axillary artery and vein, fatty cysts, soft tissue and muscle. The subject is asked to lay with the arm abducted to 90 degree and the elbow flexed to 90 degree. The head of the subject should turn away from the side to be blocked. Subject is required to avoid abduction of the arm to facilitate palpation of the axillary arterial pulse and prevent stretching of the brachial plexus.

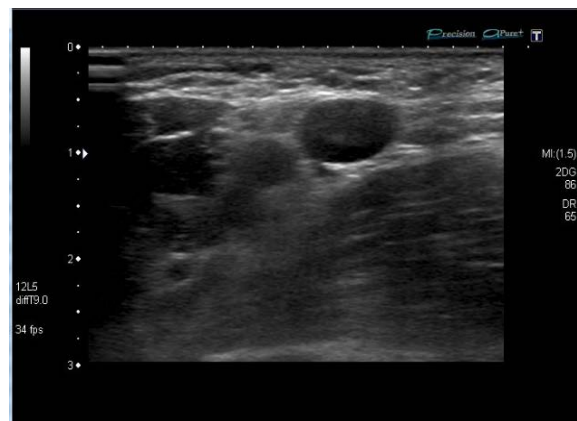


Fig. 5 Example ultrasound image of axillary region

Fig. 5 shows the example ultrasound image of the axillary region. As the image is blur due to the presence of speckle noise, assessing the image may be time consuming and subjective. Thus, pre-processing methods are implemented so the noise of this image can be minimised and make it more appropriate to be analysed.

B. Image Smoothing

Three types of filters have been tested in this experiment, namely Frost filter, Wiener filter and anisotropic filtering to smooth the high frequency speckle noise because these filters can be applied and controlled easily [19]. The definition of speckle noise is shown in equation below [16]:

$$f_{i,j} = g_{i,j}u_{i,j} + \alpha_{i,j} \quad (1)$$

After the image is obtained, two criterions are calculated for evaluating the quality of the images. The first criterion is mean square error (MSE). The mathematical definition of MSE is defined as below [26]:

$$MSE = \frac{\sum_{i=1}^M \sum_{j=1}^N |x(i,j) - \hat{x}(i,j)|^2}{MN} \quad (2)$$

The peak signal to noise ratio (PSNR) is measured for each of the filtered image. The PSNR measures the level ratio of the maximum signal power to noise power. The definition of PSNR in decibel scale is shown as below:

$$PSNR = 20 \log_{10} \left[\frac{(2^n - 1)}{\sqrt{MSE}} \right] \quad (3)$$

A higher ratio PSNR implies signal exceeds noise, indicating a better image quality. The smoothing process should be able to improve the PSNR ratio but preserve the edges in the smoothed image [20].

i. Frost Filter

Frost filter is originally derived to smooth the radar images contaminated by multiplicative noise. The Frost model develops the functional form of the minimum mean square error (MMSE) filter by utilizing locally estimated parameter values and maintains the edge structure. A localized value calculated based on the distance from the filter center, damping factor and local variance is utilized to substitute the pixel value of the image. The Frost filter is defined by the formula below:

$$DN = \sum_{n \times n} k \propto e^{-\alpha|t|} \quad (4)$$

This filter model is easy to be computed [25] and useful for improving angular edges but proved unsuitable for improving curved structures [21].

ii. Wiener Filter

Wiener filter assumes the signal and the noise are stationary linear stochastic processes and their spectral

properties are explicit. By gauging minimum mean square error (MMSE) as the performance criterion, Wiener filter deconvolves the image according to the variance of the local image to an estimation of the desired noiseless image. The filter's formula in frequency terms is expressed as below:

$$G(f) = \frac{H^*(f)S(f)}{|H(f)|^2S(f) + N(f)} \quad (5)$$

Since matched filtering methods fail to eliminate the amplitude errors and inverse filtering cannot be applied practically, the adaptive low pass Wiener filtering scheme is a better smoothing technique and is more selective in maintain edges than linear filter [22].

iii. Anisotropic Diffusion Filter

Anisotropic diffusion is a generalized process of the linear and space invariant transformation of an original image. The anisotropic diffusion filter convolves the input image with a 2D isotropic Gaussian filter, and during this diffusion process, the width of the filter will increase with the parameterized image. The anisotropic diffusion filtering scheme is proposed by Perona and Malik in 1987 and a discrete version of the Perona-Malik's Diffusion (PMD) is defined as shown in the equation below [23]:

$$I_S^{(n+1)} = I_S^{(n)} + \frac{\lambda}{|\theta_S|} \sum_{p \in \theta_S} g(\nabla I_{S,p}^{(n)}) \cdot \nabla I_{S,p}^{(n)} \quad (6)$$

C. Image Segmentation

Morphological process is performed to retain only the desired region of the image. In this project, Otsu's thresholding and manual thresholding are tested to threshold the images. Otsu's method transforms the grey level image into binary image by using the histogram shaped based image thresholding [24].

During the implementation of this transformation, the image and histogram are assumed to be bimodal and stationary. No spatial coherence is applied in the Otsu's method. Minimizing the weighted within-class variance is emphasis in order to achieve an optimum threshold value. The definition of the individual class variances are shown as below:

$$\sigma_1^2(t) = \sum_{i=1}^t [i - \mu_1(t)]^2 \frac{P(i)}{q_1(t)} \quad (7)$$

$$\sigma_2^2(t) = \sum_{i=t+1}^I [i - \mu_2(t)]^2 \frac{P(i)}{q_2(t)} \quad (8)$$

In the Otsu's thresholding, the threshold is defined as weighted sum of weighted within-class variance, which is defined as below:

$$\sigma_w^2(t) = \omega_1(t)\sigma_1^2(t) + \omega_2(t)\sigma_2^2(t) \quad (9)$$

The total variance, which is constant and independent of

time, is equal to the sum of the within class variances and the between class variance. Minimizing the within class variance is the same as maximizing the between class variance

$$\sigma^2(t) = \frac{\sigma_w^2(t) + q_1(t)[1 - q_1(t)]}{[\mu_1 - \mu_2(t)]^2} \quad (10)$$

The second attempt to threshold the images manually by selecting a suitable threshold value through trial and error. The grey scaled images contain 256 levels and all pixels below threshold value are replaced by black background. After the threshold process, the binary image will undergo inversion where the black and white pixel will be inverted to show the axillary artery and vein in white pixel for the ease of measurement in the coming part of this project. The experiment combines the erosion and dilation in the opening process.

During the opening procedure, the function smooth object contours, breaking thick connection and remove thin protrusions. During opening procedure, object smaller than the structuring element will disappear. During closing procedure, smoothed object contours join narrow break, fills long gulfs and holes smaller than the structuring element.

The level set segmentation has been applied as the segmentation method after the morphological process. Level sets represent the image object curve with an implicit surface on the pixel grid without the application of mind blogging data structures.

III. RESULT

Fig. 6 shows the original axillary region ultrasound image before being processed. The low-intensity circular shaped regions are axillary artery and vein. The smaller and lower left of the circular shaped region is the axillary artery and the larger upper right circular shaped region is the axillary vein. Surrounding the axillary artery are the muscle, soft tissue, fatty cysts and axillary nerve, which are shown in the white pixel in the sample ultrasound image.

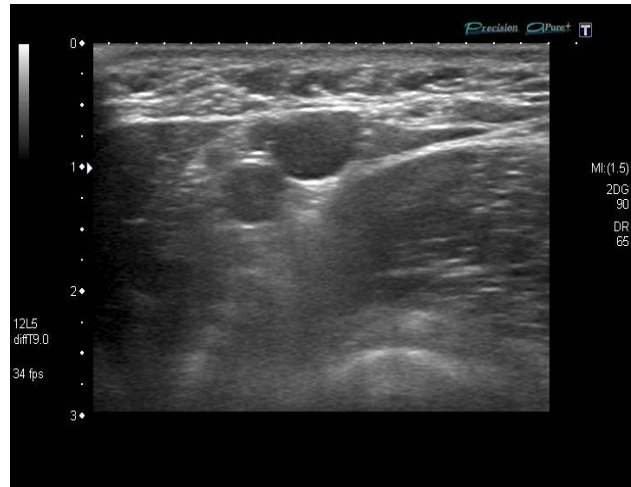


Fig. 6 Original image of axillary brachial plexus

From the obtained image, it shows that the image is contaminated with speckle noise. From the left side of the image, we can see the anechoic artifact caused by pocket of air during between the transducer and the subject. If the artifact is larger, it will cause difficulty in finding the location of axillary artery and vein.

A. Filtered Image

Three types of filters are used to improve the quality of the axillary region images. Images are input into MATLAB R2009b for the filtering process.

After the implementation of anisotropic diffusion filter, the image, shown in Fig. 7(a) indicates close-interrupted lines of the vessels after filtration. Besides, the filter reduces the noise and keeps edges of the vessel boundary. Fig. 7(b) shows reduction of noise by using Frost filter. Fig. 7(c) shows most of the edge and the structure of the vessels is preserved and speckle is removed by using the Wiener filter.



Fig. 7 Images after filtration by using (a) Anisotropic Diffusion filter, (b) Frost filter and, (c) Wiener filter

Table 1 Quality measurement of image with different filters; MSE = Mean square error; PSNR= power signal to noise ratio.

Filter Type	MSE (%)	PSNR (dB)
Frost	6.1474	16.1785
Wiener	0.0006	56.0915
Anisotropic	0.0070	45.6288

The performance of the three filters tested in this experiment has been gauged by using the MSE and PSNR. Table 1 shows the wiener filter has higher power signal to noise ratio (PSNR) and lowest mean square error (MSE) compared to anisotropic and frost filter. Wiener filtered image has better performance than the anisotropic and frost filter.

B. Image Threshold

The manual threshold converts grayscale images into binary images of all three filters. The results are shown in Fig. 8. The objective of manual thresholding is to isolate the vessels from the surrounding by selecting suitable threshold value. Different values are manually chosen by trial and error. The suitable threshold value of vessels using different filtered images is 0.3. A comparison has been made by using Otsu's method. The results are shown in Fig. 9. It is concluded that the vessel is not isolated completely and there is no clear boundary of the artery as there is still some noise persists when using the Otsu's method. Thus, the manual thresholding is selected from the two thresholding methods. Although Wiener filter shows better filtering effect, the processed images after segmentation show anisotropic diffusion filtered and manual segmentation are the best combination of pre-processing technique in this experiment.

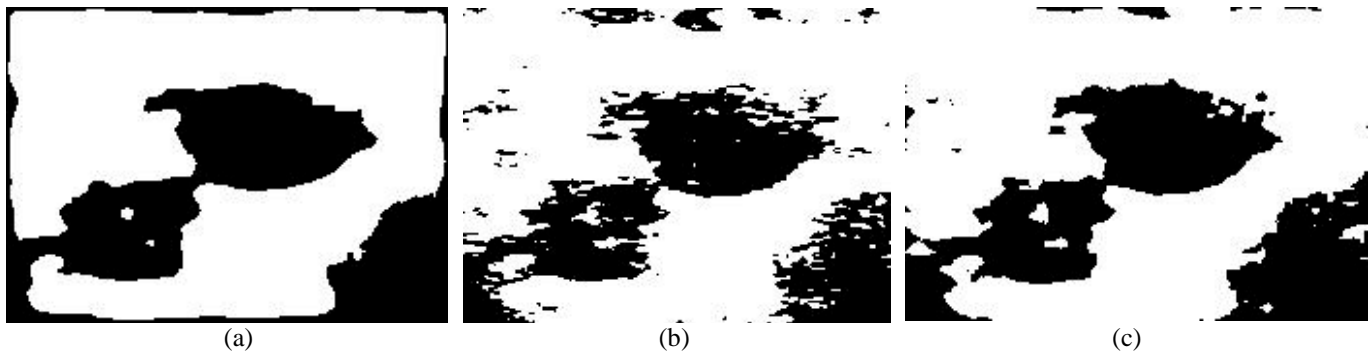


Fig. 8 Image after manually threshold value (a) Anisotropic Diffusion filtered image, (b) Frost filtered image and, (c) Wiener filtered image

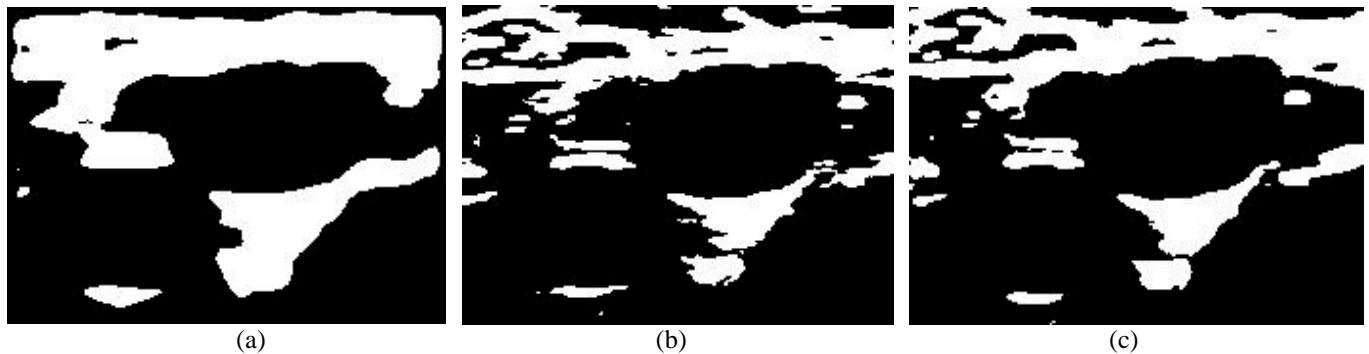


Fig. 9 Image after Otsu's method (a) Anisotropic Diffusion filtered image, (b) Frost filtered image and, (c) Wiener filtered image

C. Morphological Operation

The image is inverted after the segmentation method, which is shown in Fig. 10(a). Fig. 10(b) shows the image of artery and vein after repeating step of opening. The first step use radius less than 5 pixels by opening it with the disk-shaped structuring element while last step use ball-shaped structuring element with radius of 15 and height of 5.

The opening is a combining of erosion followed by dilation. It can remove white are around the line of the vessel with black regions. The artery and the vein shape become smoother. The size of artery region had been separated from other region.



Fig. 10 Image of artery and vein after morphological operation
(a) Inverted image (b) Opening image

D. Level Set Segmentation

Fig. 11(a) show the image of artery that is specified for initial contour region for level set method. Using level set method it exploit the fact that curves moving under their curvature smooth out and disappear, so the larger white area of axillary vein disappear and only show the axillary artery.

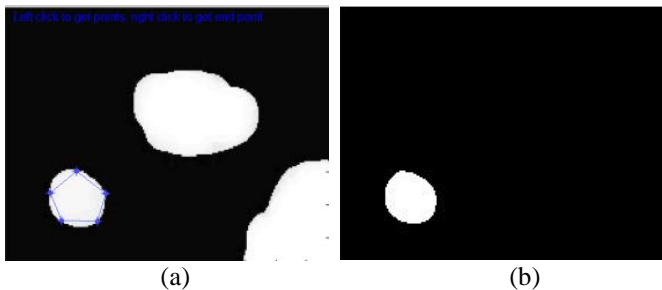


Fig. 11 Level set segmentation (a) Initial contour region of artery (b) Interest region of artery after segmentation.

After segmentation, the diameter of the axillary artery is measured. Five trials are carried out on five different images. The mean and standard deviation are calculated for the results obtained from images before and after being processed.

Table 2 Diameter measurements of axillary artery from original ultrasound images.

No of trial	Original Diameter (mm)	Mean (mm)	Standard Deviation (mm)
1	21.17	21.17	0.045
2	21.23		
3	21.10		
4	21.15		
5	21.20		

Table 3 Diameter measurements of axillary artery after the images undergo the processing methods.

No of trial	Final Diameter (mm)	Mean (mm)	Standard Deviation (mm)
1	8.99	8.99	0.019
2	9.02		
3	8.97		
4	8.98		
5	9.01		

The standard deviation results in Table 2 and Table 3 shows that images after processing technique can improve the precision of the diameter measurement since the standard deviation before standard deviation stands at 0.045 mm while after processing the image, the standard deviation falls to 0.019 mm. Furthermore, the large difference between these two set of data shows that soft tissue and muscle may be taken into calculation when measuring the axillary artery diameter from the unprocessed images.

IV. CONCLUSION

In this project, the locations of the axillary artery and vein have been shown clearly after the image undergoes through the anisotropic diffusion and morphological process. After that, measurement of the axillary artery diameter before and after the image processing procedures indicate that the latter can produce more precise axillary diameter parameter for researches on physiological effect of nerve block. As a result, the diameter parameter can further improve the accuracy of related clinical studies. In the future, the study should concentrate on expanding the subject numbers and obtaining optimal threshold values for the segmentation method. The motivation of this recommendation is to increase the reliability of the study and preserve as much as possible important information of the ultrasound image during the processing procedures.

ACKNOWLEDGMENT

The authors would like to express our thanks to Universiti Teknologi Malaysia and the Biotechnology Research Alliance for supporting and funding this study. Our appreciation also goes to the Advanced Diagnostics and E-Health Research Group members for their ideas and comments on this paper.

REFERENCES

- [1] Satapathy, A. R. and D. M. Coventry, Axillary Brachial Plexus Block, *Anesthesiology Research and Practice*, 2011, pp. 1-5.
- [2] Peter Marhofer, C. N. e., Christian Sitzwohl, and Stephan Kapral, Magnetic Resonance Imaging of the Distribution of Local Anesthetic During the Three-In-One Block, *Regional Anesthesia and Pain Management*, Vol. 90, 2000, pp. 119 – 124.
- [3] Anahi Perlas, V. W. S. C., and Martin Simons, Brachial Plexus Examination and Localization Using Ultrasound and Electrical Stimulation, *Anesthesiology Research and Practice*, Vol. 99, No. 2, 2003, pp. 429 – 435.
- [4] Rogai, L. B. a. F., A Genetic Fuzzy Rules Learning Approach for Unseeded Segmentation in Echography, *Evo Application*, 2012, pp. 305–314.
- [5] Jung-Ha An, P. B., and Steven Damelin, Identification of Nerves in Ultrasound Scans Using a Modified Mumford-Shah functional and Prior Information, *Proceedings of the World Congress on Engineering and Computer Science 2011*, Vol. I, 2011.
- [6] Amandeep Kaur, K. S., Speckle Noise Reduction by using Wavelets, *NCCI 2010 -National Conference on Computational Instrumentation*, 2010, pp. 198 – 203.
- [7] T. M. Perris and J M. Watt, The Road to Success: A Review of 1000 Axillary Brachial Plexus Blocks, *Anaesthesia*, Vol. 58, 2003, pp. 1220 – 1234.
- [8] Eko Supriyanto, Nurul Afiah Tahir and Syed Mohd Nooh, Automatic Ultrasound Kidney's Centroid Detection System, *Recent Researches in Computer Science*, pp. 160 – 165.

- [9] Ali Rafiee, Novel Intelligent Edge Detector for Sonographical Images, Proceedings of the 5th WSEAS Int. Conf. on Artificial Intelligence, Knowledge Engineering and Data Bases, 2006, pp. 280 – 285.
- [10] Stephen M. Klein, Holly Evans, Karen C. Nielsen, Marcy S. Tucker, David S. Warner, and Susan M. Steele, Peripheral Nerve Block Techniques for Ambulatory Surgery, *Anesth Analg*, Vol. 101, 2005, pp. 1663 – 1676.
- [11] Paul H. Ting and John G. Antonakakis, Evidence-based Review of Ultrasound Imaging for Regional Anesthesia, *Seminars in Anesthesia, Perioperative Medicine and Pain*, Vol. 26, 2007, pp. 218 – 228.
- [12] Robert L. Lennon and John W. Linstromberg, Brachial Plexus Anesthesia and Axillary Sheath Elastance, *Anesth Analg*, Vol. 62, 1983, pp. 215 – 217.
- [13] Vincenzo Gemignani, Francesco Faita, Lorenzo Ghiadoni, Elisa Poggianti, and Marcello Demi, A System for Real-Time Measurement of the Brachial Artery Diameter in B-Mode Ultrasound Images, *IEEE Transactions on Medical Imaging*, Vol. 26, 2007, pp. 393 – 404.
- [14] John J Badal, Annie Kiesau and Patrick Boyle, Effects of Median Nerve Block on Radial Artery Diameter and Peak Velocity, *Local and Regional Anesthesia*, Vol. 3, 2010, pp. 5 -10.
- [15] Su Cheol Kang and Seung Hong Hong, Experimental and Theoretical Analysis of Wavelet-Based Denoising Filter for Echocardiographic Images.
- [16] R.Vanithamani, G.Umamaheswar, M.Ezhilaras, Modified Hybrid Median Filter for Effective Speckle Reduction in Ultrasound Images, *Recent Advances in Networking, VLSI and Signal Processing*.
- [17] Judith G. Thomas, Richard Alan Peters and Philippe Jeanty, Automatic Segmentation of Ultrasound Images Using Morphological Operators, *IEEE Transactions on Medical Imaging*, Vol. 10, No. 2, 1991, pp. 180 – 186.
- [18] Dandan Li, Yi Shen, Zhiyan Liu and Ping He, A New Adaptive Morphological Algorithm for Contour Extraction on Ultrasound Image, *Instrumentation and Measurement Technology Conference*, 2004, pp. 2077 – 2081.
- [19] Pierrick Coupé, Pierre Hellier, Charles Kervrann, and Christian Barillot, Nonlocal Means-Based Speckle Filtering for Ultrasound Images, *IEEE Transactions on Image Processing*, Vol. 18, No. 10, 2009, pp. 2221 – 2229.
- [20] Eko Supriyanto, Wan Mahani Hafizah, Yeoh Jing Wui, Adeela Arooj, Automatic Non Invasive Kidney Volume Measurement Based On Ultrasound Image, *Recent Researches in Computer Science*, pp. 387 – 392.
- [21] B.Priestly Shan and M.Madheswaran, Generalized Despeckling Filter for Enhancing Fetal Structures to Aid Automated Obstetric Pathologies, *International Journal of Computer Theory and Engineering*, Vol. 2, No. 3, 2010, pp. 445 – 453.
- [22] Li-Hong Juang and Ming-Ni Wu, Image noise reduction using Wiener filtering with pseudo-inverse, *Measurement*, Vol. 43, 2010, pp. 1649–1655.
- [23] Takanori Koga, Eiji Uchino, Noriaki Suetake, Genta Hashimoto, Takafumi Hiro and Masunori Matsuzaki, Edge-Preserved Smoothing Method with Special Reference to Intravascular Ultrasound Image Using Anisotropic Diffusion Filter Controlled by Weighted Separability Measure, *Proceedings of the 7th WSEAS International Conference on Circuits, Systems, Electronics, Control and Signal Processing*, 2008, pp. 87 – 92.
- [24] S. Rahnamayan, H.R. Tizhoosh, and M.M.A. Salama, *Lecture Notes in Computer Science*, SpringerLink, 2005.
- [25] Victor S. Frost, Josephine Abbott Stiles, K. S. Shanmugan and Julian C. Holtzman, A Model for Radar Images and Its Application to Adaptive Digital Filtering of Multiplicative Noise, *IEEE Transactions on Pattern Analysis and Machine Intelligence*, Vol. PAMI-4, No. 2, 1982, pp. 157 – 166.

V. BIOGRAPHIES

Eko S. received his B.E in Electrical Engineering and M.E. in Biomedical Engineering from Institute Teknologi Bandung, Indonesia. He also received his PhD in Biomedical Engineering from Hamburg University, Germany. Currently he is Associate Professor in the faculty and Head of Department of Clinical Science and Engineering, Universiti Teknologi Malaysia. His fields of interests are Ultrasound Diagnostic and Therapeutic, Prenatal Diagnosis, Medical Electronics, Health Care Management and Information System, Dialysis & Medical Imaging

K. W. Lai received his B.E in Biomedical Engineering from Universiti Teknologi Malaysia. He received his PhD in Biomedical Engineering from Universiti Teknologi Malaysia and Ilmenau University of Technology, Germany under PhD Sandwich Program. Currently he is a postdoctoral researcher in Biotechnology Research Alliance, Universiti Teknologi Malaysia. He has authored over than 30 international journals and books, and he was actively involved in the Board of Editorial and Reviewer for more than 25 international journals and conferences. His research interests are including Ultrasound imaging, medical image processing, 3D reconstruction and visualization, biomedical instrumentations and surgical tool navigation.

F. S. Rino was borned at Pekanbaru, Indonesia in 1989. He received his B.E. in Electrical Engineering from Bandung Institute of Technology on 2012. Currently he is pursuing his master studies in Biomedical Engineering at Universiti Teknologi Malaysia. His research interests are electrical control and medical robot development.